

Vibration compensation for high speed scanning tunneling microscopy

D. Croft and S. Devasia^{a)}

University of Utah, Department of Mechanical Engineering, 50 South Central Campus Drive, Room 3201, Salt Lake City, Utah 84108

(Received 19 April 1999; accepted for publication 24 August 1999)

Low scanning speed is a fundamental limitation of scanning tunneling microscopes (STMs), making real time imaging of surface processes and nanofabrication impractical. The effective scanning bandwidth is currently limited by the smallest resonant vibrational frequency of the piezobased positioning system (i.e., scanner) used in the STM. Due to this limitation, the acquired images are distorted during high speed operations. In practice, the achievable scan rates are much less than 1/10th of the resonant vibrational frequency of the STM scanner. To alleviate the scanning speed limitation, this article describes an inversion-based approach that compensates for the structural vibrations in the scanner and thus, allows STM imaging at high scanning speeds (relative to the smallest resonant vibrational frequency). Experimental results are presented to show the increase in scanning speeds achievable by applying the vibration compensation methods. © 1999 American Institute of Physics. [S0034-6748(99)00812-6]

I. INTRODUCTION

In scanning tunneling microscopes (STMs), structural vibration of the scanner leads to distortions in the acquired image during high frequency (i.e., high speed) scanning of surfaces. These structural vibrations are induced by excitation of the resonant vibrational frequencies in the STM's scanner. When the STM is used as a surface analysis instrument, some of these vibration-caused distortions in the image can be removed through postcorrections.¹ However, these distortions limit the use of STMs in both real-time visualization of surface processes and also limit their use in real-time surface modification applications such as nanofabrication.^{2,3} This article describes a method for achieving high-speed operation of STMs, by finding inputs that compensate for the induced vibrations. The method uses a model of the scanner's dynamics to find input voltages that minimize vibrations^{2,4,5} during relatively high-speed operations. The approach is applied to an experimental STM and the results verify that imaging speeds can be increased by using vibration compensation methods. Although the method is applied to a STM, it is applicable to other scanning probe techniques,⁶ such as atomic force microscopy or magnetic force microscopy.

A. High speed STMs

Although STMs have improved greatly since their initial development, they still have serious limitations due to their slow scanning speed with imaging times ranging from several seconds to minutes⁷ for most conventional systems. These slow scanning speeds are not only inconvenient, but they also make STM systems more susceptible to the effects of external vibrations and piezoelectric drift. Currently, there is also great interest in high speed STMs for several applications, such as real time imaging with STMs⁸ to determine

the dynamics and mechanisms of surface processes,^{9,10} high density data storage,¹¹ and nanofabrication.^{2,3,12}

Scanning speeds can be increased by addressing two classes of problems: improving the control of the x - y axes¹ (movements in these axes correspond to the displacement of the STM tip parallel to the sample surface as shown in Fig. 1) and improving the control of the z axis^{7,13-15} (z axis movement corresponds to changing the tip-to-sample distance as shown in Fig. 1). This article studies the x - y axis control problem and shows that significant improvements can be achieved by using vibration compensation techniques. This effort is complementary to other works aimed at improving scanning speeds, such as efforts to improve control in the z axis^{13,16} and advances in high speed electronics.¹⁴

B. Scanning speed limitations

The x - y scanning speed in STM systems is limited by the smallest resonant vibrational frequency of the scanner. As the scanning speed is increased (relative to the smallest resonant vibrational frequency), the scanning movement excites the vibrational modes of the scanner and causes unwanted vibrations. These induced vibrations result in image distortions and limit the maximum scanning frequency of the STM. In practice, the achievable scan speed is substantially smaller (around 100 times smaller) than the smallest resonant vibrational frequency due to excitation of vibrations during turnarounds^{2,17} in the scanning motion.

STM scanning speeds are currently increased by either using feedback control techniques to increase bandwidth or by using piezoactuators with higher resonant vibrational frequencies. Though the use of feedback control improves linearity, turnaround transients due to velocity changes in the scan path substantially limit the maximum scan rates achieved.^{1,17} Furthermore, feedback (with the required resolution) may not be available for controlling the x - y axes in all STM systems. An alternative approach to increase the scan-

^{a)}Electronic mail: santosh@eng.utah.edu

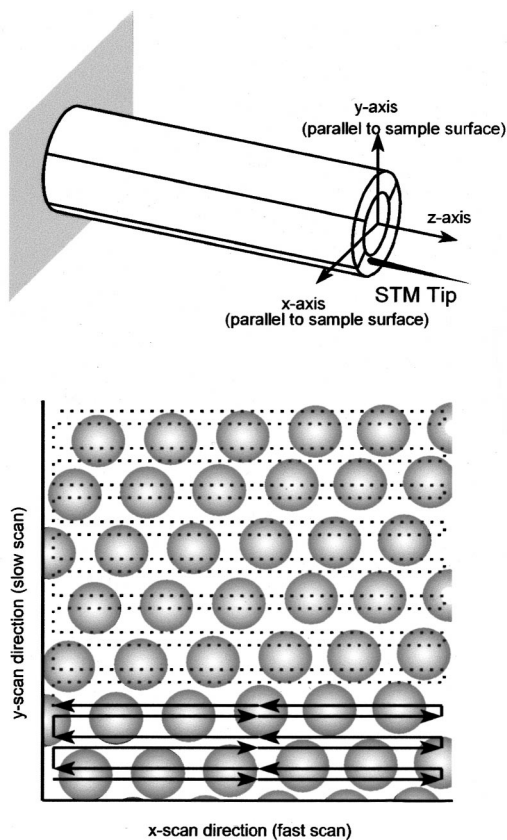


FIG. 1. Sectored-tube piezoactuator and raster scan pattern. The x - y axes of the sectored-tube piezoactuator (top) correspond to displacements parallel to the sample surface and the z -axis changes the tip-to-sample distance. A raster scan pattern (bottom) is used to collect surface data.

ning speed is to use piezoactuators with a fast dynamic response (i.e., vibrational resonance occurs at a higher frequency). Faster dynamic response can be achieved by using shorter piezotubes or by using piezoactuator configurations such as piezoplate scanners.¹⁸ However, these methods tend to limit the scanning range of the system. In addition, it is noted that although the scanning frequency is larger because the resonant vibrational frequencies are larger, the scanning speed is still limited to about 1/100th the smallest resonant frequency of the scanner. In summary, scanning speeds in STMs are significantly limited by induced vibrations in the scanner.

This article describes an inversion-based output-tracking approach^{19–21} that models the vibrational dynamics of the scanner and then uses the model to compensate for vibrations, thereby achieving imaging at relatively high scanning frequencies. Such inversion-based approaches can be used when precision tracking of a particular output trajectory (like surface scanning) is required, and are also applicable to general piezoelectric scanners.² Inversion-based approaches can also be used to account for hysteresis nonlinearities of piezoelectric scanners when long range displacements are needed.⁴ Furthermore, they have been extended to optimally modify the scan paths to account for modeling errors, input magnitude limits, and input bandwidth restrictions.^{5,22} In addition, these methods can be used in conjunction with feedback-based techniques (if feedback is available) to fur-

ther increase scanning speeds² and robustly account for modeling uncertainties.²³ In the present article, inversion-based methodology is applied to a STM scanner and experimental results showing imaging at relatively high scanning speeds are presented.

In this article, the formulation and solution of the general inversion-based vibration-compensation problem are presented in Sec. II. The effects of vibrations on STM images are studied through simulations and verified experimentally in Sec. III. This section also describes the improvements achieved by vibration compensation.

II. VIBRATION COMPENSATION

The goal of an inversion-based approach, as applied to a STM scanner, is to find inputs that compensate for induced vibrations and thereby achieve the desired scanning trajectory. The vibration compensating input to the scanner is found through the following three steps: (a) modeling the vibrational dynamics of the scanner; (b) determining the inverse model of the vibrational dynamics; and (c) using the inverse model to find inputs that will achieve the desired scanning by compensating for induced vibrations. These three steps are presented below. We begin with a description of the experimental STM system used in this work.

A. Modeling of experimental system

The experimental STM system studied in this article was a Burleigh Metris-1000 STM, which uses a sectored piezotube actuator (see Fig. 1) to position the tunneling probe. Although the work in this article uses a sectored piezotube actuator, the inversion-based vibration compensation theory is general²² and can be applied to other scanners such as those which use a different linear piezoactuator for each of the x , y , and z motions. For the scanning pattern used in this article (described in Sec. III A), the movements in the y direction were low speed, with frequency components much smaller than the smallest resonant vibrational frequency in the y direction. Thus, the slow movements in the y direction did not lead to significant vibrations and were not considered in the study.

The vibrational dynamics of the scanner (in the x direction) were modeled experimentally using a dynamic signal analyzer (DSA) (HP3650A). The vibrational dynamics were constructed by first applying a sinusoidal command voltage u of increasing frequency from the DSA to the scanner in the x direction. The vibrational response of the scanner was then measured using an inductive sensor. The measured output signal S_{output} from the inductive sensor was then returned to the DSA. The resulting input-output responses (magnitude and phase responses) at different input frequencies²⁴ are shown as Bode plots in Fig. 2. The Bode plots were then used to construct a model of the scanner described in terms of the following transfer function (in the Laplace domain)

$$\frac{S_{\text{output}}(s)}{u(s)} = \frac{2.035 \times 10^5 (s^2 - 1.07 \times 10^5 s + 4.98 \times 10^9)}{(s + 6.28 \times 10^3)^2 (s^2 + 1.80 \times 10^3 s + 6.30 \times 10^8)}, \quad (1)$$

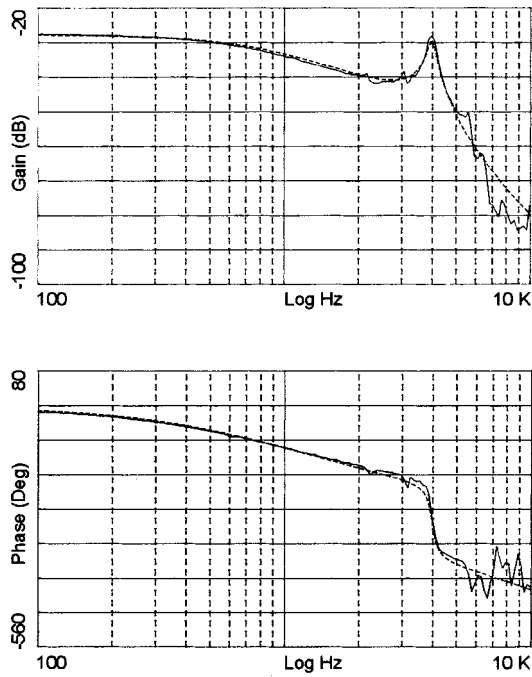


FIG. 2. Bode plots of the STM scanner. The model captures the system behavior up to the first vibrational frequency of 4000 Hz. (The solid lines represent the response of the experimental system and the dashed lines represent the response of the model.)

where $S_{\text{output}}(s)$ is the Laplace transform of the output voltage measured by the inductive sensor and $u(s)$ is the input voltage applied to the scanner. The transfer function relating the command voltage u applied to the scanner and the actual displacement x (in angstroms) of the scanner was then calibrated and found as

$$\frac{x(s)}{u(s)} = \frac{1.13 \times 10^7 (s^2 - 1.07 \times 10^5 s + 4.98 \times 10^9)}{(s + 6.28 \times 10^3)^2 (s^2 + 1.80 \times 10^3 s + 6.30 \times 10^8)}$$

$$= \frac{n(s)}{d(s)}. \tag{2}$$

Using this model [Eq. (2)], an inversion-based approach can now be used to determine the vibration-compensating inputs that achieve tracking of a desired scan path x_d .

B. Optimal inversion-based approach for improved positioning

As opposed to an exact inversion approach^{2,4} that finds inputs to exactly track a desired scan path (modulo modeling errors), a recently developed theory for optimal inversion^{5,22} was used to determine the inputs. The optimal inverse sacrifices the exact tracking requirement in order to achieve other goals, such as reduction of the input bandwidth and amplitudes, and to reduce the effects of modeling uncertainties.

This optimal inversion problem is posed as the minimization of the following objective functional:

$$J(u) = \int_{-\infty}^{\infty} \{u^*(j\omega)R(j\omega)u(j\omega) + [x(j\omega) - x_d(j\omega)]^* \times Q(j\omega)[x(j\omega) - x_d(j\omega)]\} d\omega, \tag{3}$$

where the transfer function of the vibrational dynamics [Eq. (2)] has been converted into the frequency domain by replacing the Laplace variable s in Eq. (2) with the complex frequency $j\omega$. The superscript $*$ implies conjugate transpose, and x_d is the desired output trajectory (scan path) in the frequency domain.

In this objective functional, $R(j\omega)$ and $Q(j\omega)$ are non-negative frequency dependent real-valued scalars (both should not be simultaneously zero at any frequency) that represent the weights on input u and output-tracking error $(x - x_d)$. For example, the amplitudes of the inputs can be reduced by choosing large values of R . This, however, can result in greater tracking error $(x - x_d)$. Recent works^{5,22} discuss these trade-offs in more detail. However, we point out two cases with extreme choices of R and Q . In the first case, if the weight on the scan path tracking error is zero, $Q = 0$, but R is nonzero, then the best strategy is not to track the desired trajectory at all. In the second case, if the weight on the inputs are zero, i.e., $R = 0$ but Q is nonzero then the best strategy is to exactly track the desired scan path, i.e., $x = x_d$. Thus, for the second case, the resulting optimal inverse is the exact-inverse input that achieves exact tracking of the desired scan path x_d without any modification.

For the above objective functional, the optimal inverse input⁵ u_{opt} to the scanner is given as (code available by e-mail to: santosh@eng.utah.edu)

$$u_{\text{opt}}(j\omega) = \frac{d(j\omega)}{n(j\omega)} \times \left\{ \frac{n^*(j\omega)Q(j\omega)n(j\omega)}{d^*(j\omega)R(j\omega)d(j\omega) + n^*(j\omega)Q(j\omega)n(j\omega)} \right\} x_d(j\omega). \tag{4}$$

This optimal inverse input u_{opt} is then applied to the scanner to reduce the effects of vibrations and thereby achieve high speed scanning.

III. RESULTS AND DISCUSSION

Simulations of the STM scanner were performed to study the effects of the structural vibrations in imaging, which also were experimentally verified. The vibration-compensation approach then was applied to the experimental STM system to remove the effects of the structural vibrations and to achieve high speed scanning.

Two scanning speeds were chosen to study the vibrational effects. The first scanning speed consisted of a relatively slow scanning frequency of 50 Hz which is just over 1/100th the fundamental vibrational mode (Fig. 2) of the STM scanner. The effects of structural vibrations should not be significant at this relatively low 50 Hz scanning frequency. The second (faster) scanning speed was chosen as 445 Hz, which corresponds to approximately 1/10th the fundamental vibrational mode, where the effects of the vibrational dynamics on the STM image are clearly visible. Descriptions of the scan pattern and x -scan path used are given below. The simulation results also are presented, as are the experimental results.

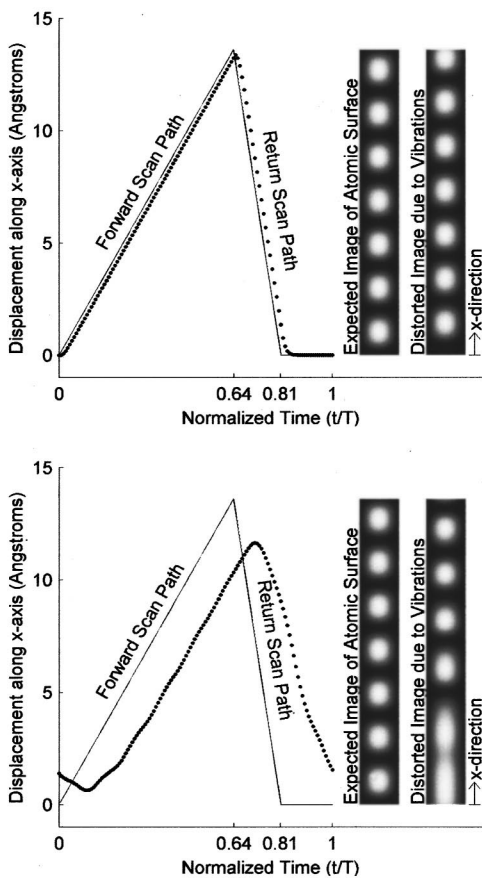


FIG. 3. Simulated scan paths and images. (The solid lines represent the desired scan path while the dotted lines represent the achieved scan paths.) For relatively slow scan rates, such as 50 Hz (top), the scanner's dynamics have little effect. For faster scan rates, such as 445 Hz (bottom), the scanner's dynamics significantly affect the achieved scan path, causing distortions in the surface image. (Note: T represents the time for one complete scan cycle.)

A. Raster scan pattern

The standard scan pattern used to image sample surfaces in STMs is the raster pattern (Fig. 1). For a fixed y displacement, the x displacement varies and the tunneling current is measured at different positions along the x -scan path. Since position information is not available, the tunneling current is measured at a constant sampling rate. Once a complete scan in the x direction is finished, the y displacement is incremented, and the process is repeated. Thus, the x -scan path chosen (Fig. 3) consists of the following three time segments: (a) a forward scan where the z -axis data is collected (the tunneling current is measured) at a constant sampling rate; (b) a quicker return scan path where no z -axis data is collected; and (c) a short time interval where the x displacement remains constant while the y displacement is incremented. Although the results presented are for this particular scan path, the proposed inversion-based vibration-compensation approach is applicable to other scan paths as well.

B. Simulation results

To study the effects of vibrations on the imaging capabilities of the STM, simulations were performed. Low- and

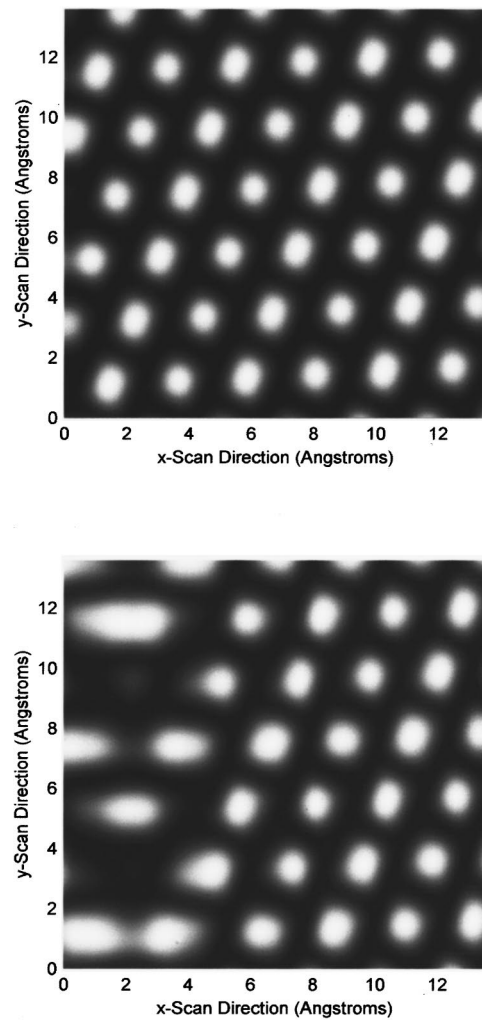


FIG. 4. Simulated surface images without vibration compensation. For relatively slow scan rates, such as 50 Hz (top), the scanner's dynamics do not significantly affect the surface image. For faster scan rates, such as 445 Hz (bottom), the scanner's dynamics significantly affect the surface image.

high-frequency scanning were simulated. At low scan frequencies, the vibrational effects are small and the relation between the x displacement x of the scanner and the applied input u can be approximated by the following expression:

$$x = ku, \tag{5}$$

where $k = 2.26 \text{ \AA/v}$ is the low frequency gain of the scanner found by setting $s = 0$ in Eq. (2) and u is the input voltage to the scanner. Thus the input that achieves the desired scan path x_d (Fig. 3), can be found as

$$u(t) = \frac{1}{k} x_d(t). \tag{6}$$

This input does not consider the dynamic vibrations in the STM system. Therefore, the achieved scan path will differ from the desired scan path. This difference between the achieved and desired scan paths can be significant at high-speed scanning.

Simulations were performed (using MATLAB²⁵) by applying inputs which were found without accounting for the vibrations [Eq. (6)]. The simulated scan path and the desired

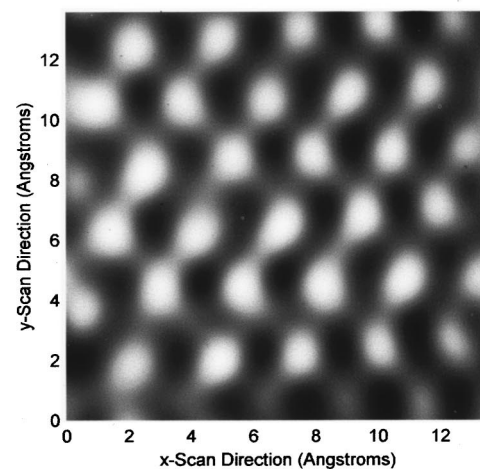
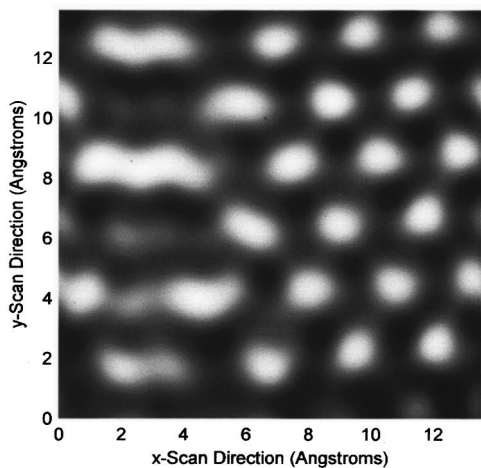
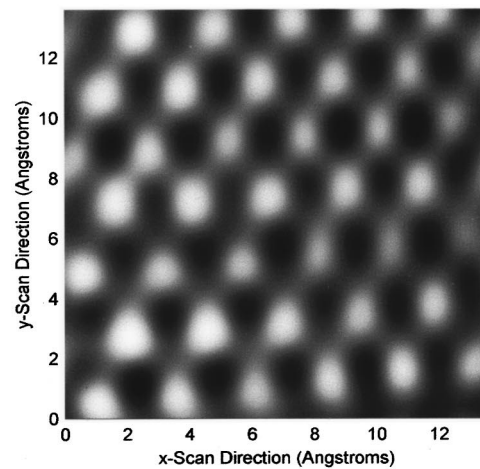
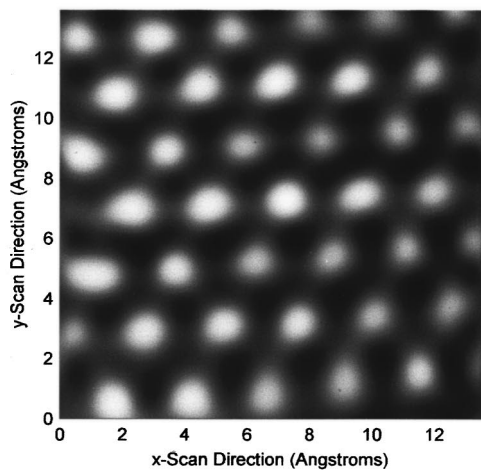


FIG. 5. Experimental surface images without vibration compensation: 50 Hz scan rate (top) and 445 Hz scan rate (bottom).

FIG. 6. Experimental surface image with vibration compensation: 50 Hz scan rate (top) and 445 Hz scan rate (bottom). Compare this with Fig. 5.

scan path are shown in Fig. 3 for a low frequency (50 Hz) input trajectory and a high frequency (445 Hz) input trajectory. Simulated STM images of a single row of atoms for a highly oriented pyrolytic graphite (HOPG) surface also are depicted in this same figure. Larger simulated surface scans of the same atomic surface are shown in Fig. 4. The distortions appear in these simulations due to the deviations of the achieved scan path from the desired scan path caused by the vibrations.

As seen in Figs. 3 and 4, the effects of the vibrational dynamics are negligible at the low scanning rate of 50 Hz. However, at the higher scanning rate of 445 Hz the vibrational dynamics significantly affect the x -scan path and simulations show a significantly distorted image. This is due to the fact that the achieved scan path deviates significantly from the desired scan path for the higher input trajectory of 445 Hz (Fig. 3). For example, the initial portion of the achieved scan path actually is in the wrong direction in the initial portion of the scan (Fig. 3), thereby resulting in a blurred image. After the achieved scan path turns and the tunneling tip moves in the correct direction, there still is a large time delay between the achieved scan path and the desired scan path. In addition to this lag in the scan path,

there also is a large discrepancy between the desired scan path amplitude and the achieved scan path amplitude (Fig. 3).

C. Experimental results

To verify the simulation results and demonstrate how the inversion-based approach can be used to compensate effectively for the vibrational dynamics, the experimental STM system (described in Sec. II A) was used to scan the surface of a HOPG graphite sample. In these experiments the STM was operated in the constant height mode (i.e., the z -axis feedback controls were inactive). This allowed the isolation and investigation of the vibrational effects in the x axis. All experiments were performed on the same sample with the same setup.

Two sets of experiments were performed. For the first set, the inputs that do not compensate for vibrations [found using Eq. (6)] were applied to the STM scanner, first, at a 50 Hz scanning rate, and second, at a 445 Hz scanning rate (shown in Fig. 5). These experimental images are similar to the simulation results shown in Fig. 4. Second, the inputs determined using the inversion-based vibration-compensation approach [Eq. (4)] were applied to the experi-

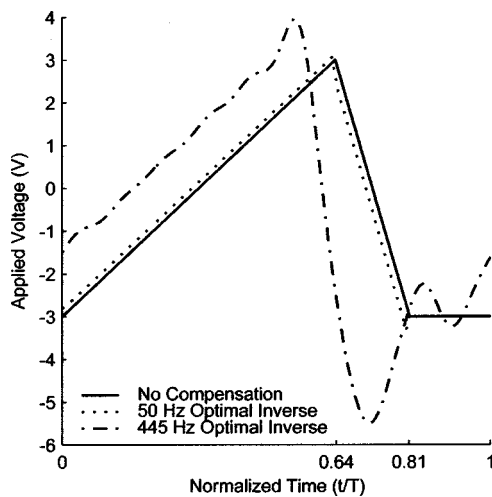


FIG. 7. Inputs used to compensate for the vibrations.

mental system and the resulting images are shown in Fig. 6. As seen from these figures, the effects of the vibrational dynamics have been effectively removed (compare Figs. 5 and 6) by the use of the vibration compensation approach and high speed scanning is achieved. The inputs used to compensate for the vibrations are shown in Fig. 7.

The simulation results and experimental results demonstrate that high-speed scanning can be achieved by using inputs that compensate for vibrations. Even at the relatively low scanning rate of 50 Hz, the optimal inversion-based approach improved the imaging of the STM system. In the experimental surface image shown in Fig. 5, a slight blurring or stretching of the image occurs along the left hand side, often referred to as *tip drag*. This tip drag effect, although relatively small at 50 Hz, has been removed from the 50 Hz image by the inversion-based vibration compensation approach (compare Figs. 5 and 6).

The distortions in the STM image due to vibrations are significant at the higher scanning frequency of 445 Hz as shown in the simulated STM image (Fig. 4) and verified by the experimental STM image (Fig. 5). These distortions in the image at the 445 Hz scanning rate have been removed using the inversion-based vibration-compensation approach, as shown in Fig. 6. Therefore, the inversion-based approach can be used to achieve STM imaging at significantly higher scan rates (relative to smallest vibrational frequency of the scanning system). Thus, the inversion-based approach allows the STM to be used in high speed scanning for real-time imaging of dynamic effects and for STM-based nanofabrication.

It is noted that the scanning speed of the STM system used in the experiments was limited to 445 Hz due to hard-

ware considerations (computational and data acquisition overheads). Related previous works^{2,4,5} on general piezoelectric scanning systems have demonstrated that scanning is possible at scanning frequencies near the fundamental vibrational frequency of the scanner. Our current research is aimed at extending the scanning in the STM system to higher speeds, approaching the first fundamental vibrational frequency, which would correspond to scan rates in the 2–4 kHz range. Other current efforts also include using hysteresis compensation for large range scanning and the integration of the vibration-compensation approach for high-speed x - y scanning with improvements in the z -axis controls.

ACKNOWLEDGMENTS

This work was supported by NSF Grant Nos. DMI 9612300 and CMS 9813080. The authors would like to thank Carol Rabke and Gordon Shedd for the help they provided in the instrumentation of the scanning tunneling microscope.

- ¹R. Barrett and C. Quate, *Rev. Sci. Instrum.* **62**, 1393 (1991).
- ²D. Croft, D. McAllister, and S. Devasia, *J. Manuf. Sci. Eng.* **120**, 617 (1998).
- ³E. Snow, P. Campbell, and F. Perkins, *Proc. IEEE* **85**, 601 (1997).
- ⁴D. Croft and S. Devasia, *AIAA J. Guid. Control Dyn.* **21**, 710 (1998).
- ⁵D. Croft, S. Stilson, and S. Devasia, *Nanotechnology* **10**, 201 (1999).
- ⁶R. Wiesendanger, *Scanning Probe Microscopy and Spectroscopy* (Cambridge University Press, Cambridge, 1994).
- ⁷H. Mamin, H. Birk, P. Wimmer, and D. Rugar, *J. Appl. Phys.* **75**, 161 (1994).
- ⁸A. Bryant, D. Smith, and C. Quate, *Appl. Phys. Lett.* **48**, 832 (1986).
- ⁹F. Besenbacher *et al.*, *J. Vac. Sci. Technol. B* **9**, 874 (1991).
- ¹⁰C. Nakakura *et al.*, *Rev. Sci. Instrum.* **69**, 3251 (1998).
- ¹¹S. Hosaka *et al.*, *Nanotechnology* **8**, A58 (1997).
- ¹²C. Marrian and E. Snow, *Microelectron. Eng.* **32**, 173 (1996).
- ¹³S. Hosaka, T. Hasegawa, S. Hosoki, and K. Takata, *Rev. Sci. Instrum.* **61**, 1342 (1990).
- ¹⁴D. Botkin *et al.*, *Rev. Sci. Instrum.* **66**, 4130 (1995).
- ¹⁵R. Curtis, T. Mitsui, and E. Ganz, *Rev. Sci. Instrum.* **68**, 2790 (1997).
- ¹⁶D. Scholl, M. Everson, R. Jaklevic, and W. Shen, *Rev. Sci. Instrum.* **63**, 4046 (1992).
- ¹⁷N. Tamer and M. Dahleh, in *Proceedings of the 33rd Conference on Decision and Control* (IEEE, Lake Buena Vista, FL, 1994), Vol. 32, p. 1826.
- ¹⁸R. Koops and G. Sawatzky, *Rev. Sci. Instrum.* **63**, 4008 (1992).
- ¹⁹S. Devasia, D. Chen, and B. Paden, *IEEE Trans. Autom. Control* **41**, 930 (1996).
- ²⁰L. Silverman, *IEEE Trans. Autom. Control* **63**, 4046 (1969).
- ²¹R. Hirschorn, *IEEE Trans. Autom. Control* **24**, 855 (1979).
- ²²J. Dewey, K. Leang, and S. Devasia, *J. Dyn. Syst., Meas., Control* **120**, 456 (1998).
- ²³Y. Zhao and S. Jayasuriya, *J. Dyn. Syst., Meas., Control* **117**, 490 (1995).
- ²⁴N. Nise, *Control Systems Engineering* (Benjamin/Cummings, Redwood City, CA, 1992).
- ²⁵Matlab, The Mathworks, Inc., 1984-1998.